Bulletin of Earthquake Engineering (2021) 19:1739–1763
https://doi.org/10.1007/s10518-020-01037-1

ORIGINAL ARTICLE

Seismic risk and loss estimation for the building stock in Isfahan: part II—hazard analysis and risk assessment

Mohsen Kohrangi[1] · **Paolo Bazzurro**[2] · **Dimitrios Vamvatsikos**[3]

Received: 23 June 2020 / Accepted: 29 December 2020 / Published online: 26 January 2021

Abstract

The second part of a seismic risk assessment study for the Iranian city of Isfahan is presented, focusing on the description of the hazard, the risk analysis, and the discussion of the results. This study utilizes the building exposure model, the fragility and the vulnerability curves illustrated in the companion paper. The earthquake occurrence source model adopted is based on the EMME14 hazard study. The site effects accounting for the soil nonlinear behavior are modeled by means of a Vs_{30} map derived from the topographical slope. The validity of this map is tested based on the local surface geology and geotechnical reports. The probabilistic seismic hazard maps for different return periods that account for site effects are generated and compared with the design spectra mandated by the Iranian national seismic design code. In addition, direct seismic monetary and human losses are estimated for two earthquake scenarios and also for 100- and 475-year return periods. We show loss maps and loss curves, offering insights on the most vulnerable building classes and the spatial distribution of the estimated losses. The results provide a basis for pre- and post-disaster emergency planning, for global and local urban planning, as well as for conceiving adequate risk mitigation strategies including devising fair earthquake insurance policies. This study may also serve as a blueprint for carrying out similar work in other urban areas of the Middle East.

Keywords Urban risk assessment · Earthquake · Isfahan · Iran

Mohsen Kohrangi: Formerly at: Scuola Universitaria Superiore IUSS Pavia, Pavia, Italy.

✉ Mohsen Kohrangi
mohsen.kohrangi@redrisk.com

Paolo Bazzurro
paolo.bazzurro@iusspavia.it

Dimitrios Vamvatsikos
divamva@mail.ntua.gr

[1] RED, Risk Engineering + Development, Pavia, Italy

[2] Scuola Universitaria Superiore IUSS Pavia, Pavia, Italy

[3] School of Civil Engineering, National Technical University of Athens, Athens, Greece

1 Introduction

Many private and public stakeholders are directly or indirectly affected by the impact of earthquakes in a region. A stakeholder could be a governmental organization that needs to prepare for minimizing the impact of future events or to manage the emergency response, or it could be a private organization that has spatially distributed assets exposed to the earthquake threat. Therefore, it is crucial for such public or private organizations to first understand the level of seismic risk that their portfolios of properties are subject to in order to make appropriate decisions to mitigate it. The necessary risk estimates are provided by *regional* or *portfolio risk assessment* studies. Such studies require vast amounts of data and computations to generate a probabilistic *seismic risk model* that: (1) quantifies the likelihood and the corresponding intensity of the possible future ground motions; (2) evaluates the vulnerability of the exposed assets and people to the effects of earthquake ground motions; and (3) estimates the possible expected direct losses to structures, infrastructure, and people in areas as large as a city, an administrative region or a country. In other words, with knowledge, albeit imperfect, of the level of ground shaking at a regional or urban level one could estimate, for example, the likelihood of occurrence in a given period of time of: (1) monetary losses caused to specific structures or portfolio of structures owned by a corporation or insured by an insurance company, (2) numbers of people killed, injured, or displaced; (3) limited (or no) access to certain critical buildings, such as hospitals and police stations, because of yellow or red tagging; and (4) the interruption of critical lifelines such as power, water, and transportation networks. Since precise earthquake prediction is still unfeasible, these probabilistic damage or loss assessments are the only credible sources of information to decision makers for devising seismic risk reduction strategies in regional or urban areas.

The current paper and its companion (Kohrangi et al. 2021) describe the steps followed to create and utilize such a seismic risk assessment model for the city of Isfahan, one of the major industrial and historical cities in central Iran. The companion paper presented the procedure and the data used to generate the exposure model (which contains all residential and mixed-use buildings and most, if not all, public buildings), the fragility and the vulnerability curves, while this article focuses on the description of the seismic hazard model and illustrates the results of the seismic risk analysis. The risk assessment is conducted for two likely earthquake scenarios selected from seismic hazard disaggregation. In addition, for illustration purposes we generated and critically evaluated direct loss maps for the return periods of 100 and 475 years.

2 Existing hazard and risk assessment studies for Iran

The first national seismic design guideline of Iran was introduced and enforced after the M7.2 Buin-Zahra earthquake in 1962. Since 1987 its updated version, called the Standard 2800, was adopted as the stand-alone seismic design code of Iran. The research center of the Iranian Ministry for Road and Urban Development (BHRC) is the national organization responsible for generating and updating this standard. Different versions of the Standard 2800 have been in force in different periods of time: 1987–1998 (version 1), 1999–2004 (version 2), 2005–2011 (version 3) and 2012 to date (version 4) (ICSRDB 2014). Standard 2800 employs a seismic zonation map that indicates the level of seismicity for different

regions. A list of probabilistic seismic hazard zoning studies in Iran is provided in Zare (2015) while the procedure that resulted in the zonation map of the last version of Standard 2800 is described in Moinfar et al. (2012). Two regional hazard studies including Iran carried out by international consortia of researchers warrant a mention here. The first noteworthy initiative is the Global Seismic Hazard Assessment Program, GSHAP (Giardini 1999). This project started in 1992 and finished in 1999 with the publication of the first global seismic hazard map of peak ground acceleration (*PGA*) with a return period of 475 years. Similarly, the Earthquake Model of Middle East (EMME) project (Şeşetyan et al. 2018) developed in 2014 a regional scale harmonized seismic hazard model for eleven countries in the Middle East region (Danciu et al. 2016b). At the urban level, many studies have focused on the seismic hazard analysis of large cities such as Tehran, Shiraz, Mashhad and Qom (Abdi et al. 2013; Ghodrati Amiri et al. 2008; Jafari et al. 2005; Kamalian et al. 2008; Sadeghi et al. 2014; Shafiee et al. 2011; Zafarani et al. 2017). Two studies investigated the seismic hazard of Isfahan in terms of characterization of the active faults around the city (Beygi et al. 2016; Safaei et al. 2012) and to generate a micro-zonation *PGA* hazard map (Tajmir Riahi et al. 2014).

Several studies were dedicated to the entire process of urban risk assessment for major cities in Iran. Firstly JICA (2000) performed a seismic risk assessment for Tehran based on the building data from city blocks provided by the Iranian Census Center. Mansouri et al. (2010) used higher-resolution data at the parcel (i.e., land lot) level, including the city topography and building heights, as well as more refined vulnerability curves compared to those in JICA, to estimate the direct building losses for one district in Tehran. Zolfaghari (2010) used a catastrophe loss model of Tehran as a case study to promote the property insurance in developing countries. Mansouri et al. (2014) established a framework for earthquake risk assessment of Iran and implemented this framework for a hypothetic earthquake scenario in Tehran and two real M6.4 and M6.3 earthquakes that occurred in Ahar-Varzeghan in 2012. Sadeghi et al. (2015) performed an earthquake risk analysis in terms of monetary and human losses for a case study in one district of Shiraz. Yazdi-Samadi and Mahsuli (2018) proposed and implemented a methodology for time-variant seismic risk analysis of transportation networks in Isfahan. More recently, Motamed et al. (2019) developed a probabilistic earthquake loss model for the entire Iran at a provincial level while Firuzi et al. (2019) quantified the annualized earthquake induced losses for residential building in Tehran. This study provides a seismic risk assessment for the building stock of Isfahan where no risk assessment study is available, to the best knowledge of the authors.

3 Probabilistic seismic hazard assessment

The Iranian plateau is located between the Arabian Plate in the southeast, and the Turan Shield in the northwest (Zare 2010), being part of the Alpine-Himalayan orogenic belt. This belt is seismically active with a unique pattern of deformation. Based on the global positioning system, a deformation rate of less than 2.0 mm/year in Central Iran up to 19.5 ± 2 mm/year in the Makran subduction zone is reported by Vernant et al. (2004). Due to pressures generated by this movement, large magnitude earthquakes occur in the Iranian Plate. The seismicity history of the area around Isfahan reveals various records of historical (Ambraseys and Melville 1982) and instrumental events. In addition, more than 81 active faults are identified within 100 km of the city center. Among them, 24 faults longer than 40 km have the potential to create large magnitude events (Safaei 2005; Tajmir Riahi et al.

2014). The following subsections describe the model adopted for seismic hazard analysis, the site effects and the ground motion prediction equations (GMPEs) utilized for this study.

3.1 Seismic source model

The Earthquake Model for the Middle East[1] Project, hereafter EMME, provides a cross-border harmonized seismic hazard model for a region encompassing eleven countries, including Afghanistan, Armenia, Azerbaijan, Cyprus, Georgia, Iran, Jordan, Lebanon, Pakistan, Syria and Turkey (Danciu et al. 2016a, 2017; Erdik et al. 2012; Zare et al. 2014). Herein for our probabilistic seismic hazard analysis (PSHA) we use the EMME hazard source model, publicly available at Danciu et al. (2016b). The seismic sources in EMME are primarily active faults across the region with related information on geometry and rates of movement. Seismic source zones have been delineated and parameterized using all available data (Danciu et al. 2017). Active shallow crustal, stable continental, and deep seismicity regions as well as subduction zones (interface or in-slab) are the four tectonic environments included in the model. The last one, however, does not affect the seismic hazard of Isfahan.

Two alternative representations of the source model, namely an "area source model" and a "background seismicity and active faults model", were developed in EMME and adopted herein. The epistemic uncertainty in the source modelling approach is considered via a logic tree in which the area source model branch is weighted 60% and the background plus faults model branch is weighted 40%. The higher weight of the former reflects the better correspondence of the area source model with observed seismicity and tectonic and/or geological information. In the EMME modelling process, the borders of area sources were chosen to cover both the seismically active and inactive geological faults, while the seismic occurrence rates on each area source were extracted from a harmonized earthquake catalogue (Zare et al. 2014), both instrumental and historical. Because of the limited time span covered by the catalogue, the occurrence rates of large magnitude earthquakes might be biased especially in the area sources where several earthquake cycles may not have been observed yet.

As stated earlier, for the PSHA analysis of Isfahan we considered all seismic sources in EMME within 200 km from the center of the city. It should be noted, however, that the EMME source model was originally developed for regional rather than urban hazard and risk assessment purposes. Strictly speaking, studies at a more localized scale, such as the urban risk study here, would warrant a more detailed characterization of the faults close to the city. To date, however, EMME contains the most reliable seismogenic source model likely to produce large earthquake events (Danciu et al. 2017) close to Isfahan and, therefore, we utilized it without any modifications or improvements in our study.

3.2 Ground motion prediction equation selection

GMPEs are one of the main factors that influence the accuracy of PSHA and risk assessment results (Crowley et al. 2005). In recent years, the number of such models has significantly increased in parallel with the improvements in strong motion networks and the availability of ground-motion data (Douglas and Edwards 2016). Such variety makes selection

[1] http://www.emme-gem.org/

of the most appropriate GMPEs a scientific challenge. Various aspects such as the tectonic regime, ability to model the site effects, regional or global database utilized for the development, distance and magnitude applicability of the model should be accounted for when selecting the GMPEs. According to EMME, the three seismotectonic regions of "Active Shallow Crust", "Stable Shallow Crust" and "Deep Seismicity" are present within 200 km from the city center of Isfahan.

EMME performed a comprehensive study on selecting suitable GMPEs representative of ground motion data in the entire region of the Middle East and provided recommendations for GMPEs for each of the seismogenic regions. The coherency and rigorousness provided by the data driven technique adopted in EMME (Danciu et al. 2016a) was meant to avoid arbitrary choices. Given the few GMPEs available in the literature for stable shallow crust and deep seismicity, we use the same GMPEs suggested by EMME. For active shallow crustal regions, the model recommended using the GMPEs of ASB14 (Akkar et al. 2014), CY08 (Chiou and Youngs 2008), AC10 (Akkar and Cagnan 2010) and Zetal06 (Zhao et al. 2006). Based on a database of earthquakes specific to Iran, Fallah Tafti et al. (2017) ranked GMPEs for two distinct seismotectonic Iranian regions utilizing the three different quantitative methods of likelihood (LH), average log likelihood (LLH) and Euclidian Distance Ranking (EDR). For example, the EDR approach that we favored, identified the GMPEs of CB14 (Campbell and Bozorgnia 2014), BSA14 (Boore et al. 2014), CY14 (Chiou and Youngs 2014), ASK14 (Abrahamson et al. 2014) and Zetal06 (Zhao et al. 2006). Zafarani and Mousavi (2014) investigated the regional dependency of nine local, regional and global GMPEs with respect to 163 free-field acceleration recordings of 32 earthquakes in Northern Iran. Their results show that the best fitting models for Iran based on LH scoring indices are, in descending order, AS08 (Abrahamson and Silva 2008), CY08 (Chiou and Youngs 2008) and Getal09 (Ghasemi et al. 2009), whilst the LLH ranking identified Getal09, AS08 and CY08 instead.

The authors of the EMME GMPE selection study (Danciu et al. 2016a) emphasized that when selecting GMPEs for a site within the Middle East for use with the EMME source model, it is crucial to at least adopt four GMPEs that represent: (1) local models that describe the local characteristics of the strong-motion data, (2) pan-regional models to account for completeness of the dataset at large tectonic scale, (3) models from the Next Generation Attenuation (NGA) project due to their overall performance, complex functional forms and aleatory uncertainty models, and (4) global predictive models to enhance the data of large magnitude events. Following all these suggestions while also seeking a consensus with the aforementioned local studies for Iran, we selected the four GMPEs of Ketal15 (Kale et al. 2015), ASK14, CY14 and Cauzzi et al. (2015) with equal weights of 0.25 in the logic tree. This choice intends to represent the four categories of GMPEs suggested above.

3.3 Site effects and Vs_{30} mapping for Isfahan

The significant impact of local soil conditions on the earthquake ground motion intensity has been observed in many past events. Typically, the time averaged shear wave velocity in the upper 30 m of the soil profile (Vs_{30}) is the standard soil property utilized to characterize the seismic site conditions. Similarly to many other seismic design codes, Standard 2800 accounts for the soil effects by considering four different soil types based on Vs_{30} values, namely Type I: $Vs_{30} > 750$ m/s; Type II: $Vs_{30} = 375$–750 m/s; Type III: $Vs_{30} = 175$–375 m/s; and Type IV: $Vs_{30} < 175$ m/s. The design spectrum is accordingly modified for each soil

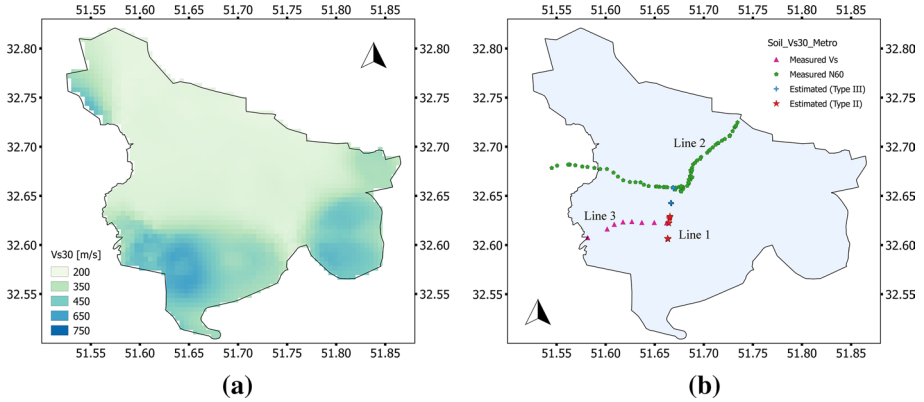

Fig. 1 **a** Spatial Vs_{30} distribution map for Isfahan developed based on the topographical slope (Wald and Allen 2007); **b** location of the subway project boreholes where geotechnical data are available

type to reflect its impact on the ground motion intensity. Nevertheless, because no Vs_{30} (or soil type) map is made available by the national code, engineers typically decide the classification of the soil based on experience or, better, on local geotechnical borehole tests. The GMPEs adopted in our study also use Vs_{30} as a proxy for modeling local site effects.

To develop aVs_{30} map for the region of interest, as customarily done for risk assessment studies for large areas we adopted the approximate method based on the *topographical slope* proposed by Wald and Allen (2007) that underpins the Vs_{30} map for Isfahan provided by the USGS.[2] Figure 1a shows the spatial distribution of the estimated Vs_{30} values from this approach. This map indicates the predominance of soil Type III (about 68% of the total area of interest) in the northern to central regions while the southern part mainly consists of soil Type II (corresponding to about 32% of the area). This spatial distribution of the soil types in the city is in agreement with the overall understanding of the local geotechnical engineering community and geological reports (Abdolahi et al. 2014) that support a gradual increase of Vs_{30} from north to the south (i.e., change from soil type III to soil type II). According to the aforementioned report, Isfahan is mainly located on Quaternary alluvial sediments and only the southern border is built on the Jurassic rock units close to the southern hills. The bedrock consists of alternating layers of "shale" and "sandstone". Alluvial formations comprise foothill alluvial sediments and fluvial deposits. The alluvial sediments of the foothills are composed of coarse-grain sediments and fine-grain filling components with different ratios. The sediments cover the bedrock surface in the southern part of the city. The fluvial deposits, which are replaced by foothill alluvial deposits along a line from south to north, consist of alternating fine-grain flood plain sediments (clay and silt) and coarse-grain turbulence sediments (sand and gravel).

In addition to the slope based Vs_{30} estimates, we use the findings of three geotechnical reports conducted for the subway project in Isfahan (i.e., Lines "1", "2" and "3" in Fig. 1b) to gauge the accuracy of the adopted slope-based approach. These reports provide soil profile data for about 130 boreholes along the subway lines and at the stations as shown in Fig. 1b. Three different type of data are available in these reports to estimate the shear wave

[2] https://earthquake.usgs.gov/data/vs30/

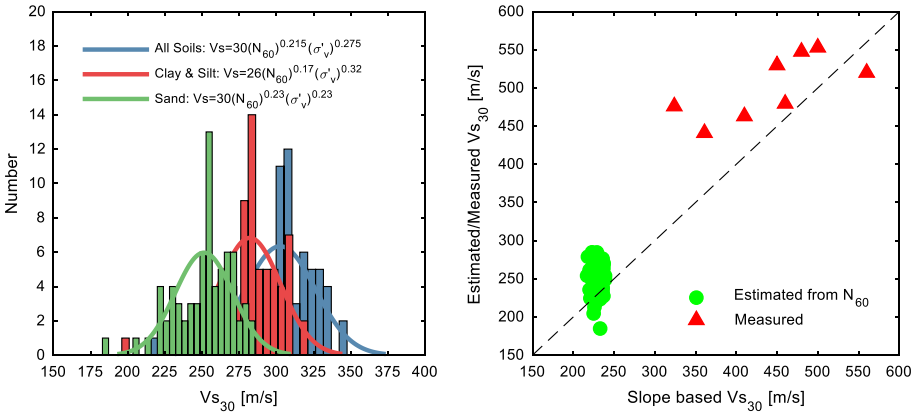

Fig. 2 **a** Histogram of the Vs_{30} estimates based on SPT blow counts (N_{60}) using three different equations adopted from Wair et al. (2012), each shown in the legend where σ'_v is the effective stress; **b** the comparison between the slope-based Vs_{30} estimates versus both the measured Vs_{30} estimates and the Vs_{30} estimated based on N_{60} for sand conditions

velocity profiles at the locations of the boreholes. The boreholes along the north–south Line 1 (see red stars and blue crosses) provide a classification of the soil type (i.e., soil type II and III) according to Standard 2800. From the tests at the locations along Line 2 (see green pentagons) we extracted the Standard Penetration Test (SPT) blow counts (N_{60}) data in the upper 30 m of the soil. In this case we used approximate equations proposed by Wair et al. (2012) to estimate the shear wave profiles and, from there, the Vs_{30} at the location of the boreholes. Given the variations of the soil types that included clay, silt and sand, we used three different equations appropriate for each soil type. Figure 2a shows the histogram of the computed Vs_{30} estimates, which range between 200 and 300 m/s for all cases corresponding to soil type III of Standard 2800, and the utilized equations in the legend. Finally, Line 3 (see magenta triangles) provides direct Vs measurements at eight boreholes in the upper 30 m of the soil surface, allowing direct estimation of Vs_{30}.

For the Line 1 case, the slope-based Vs_{30} estimates are within the range specified by the geotechnical report. Figure 2b shows a comparison between the topographical-slope-based Vs_{30} estimates versus both the measured Vs_{30} estimates (based on the report of Line 3) and the N_{60}-based estimates (based on the report of Line 2). Slope-based estimates tend to predict more homogeneous results vis-à-vis measurements, as becomes apparent for softer soils where a fairly consistent slope-based 230 m/s result is seen to correspond to measured Vs_{30} values of 180–290 m/s. Otherwise, there is a fair agreement between the geotechnical estimates and the slope-based estimates at least at the location of the boreholes considered herein. This agreement supports the credibility of the slope-based Vs_{30} map of Fig. 1a that we employ for hazard computations henceforth. Nevertheless, we emphasize that more geotechnical tests spatially distributed over the entire region of interest would be beneficial to test further the reliability of the Vs_{30} data.

Finally, it should be noted that besides the method adopted here that uses Vs_{30} as a proxy to account for site effects, there are also more precise and robust techniques to account for the nonlinear soil-site effects in probabilistic seismic-hazard analysis. One example, is the method of Bazzurro and Cornell (2004) that also accounts for the uncertainty in the soil

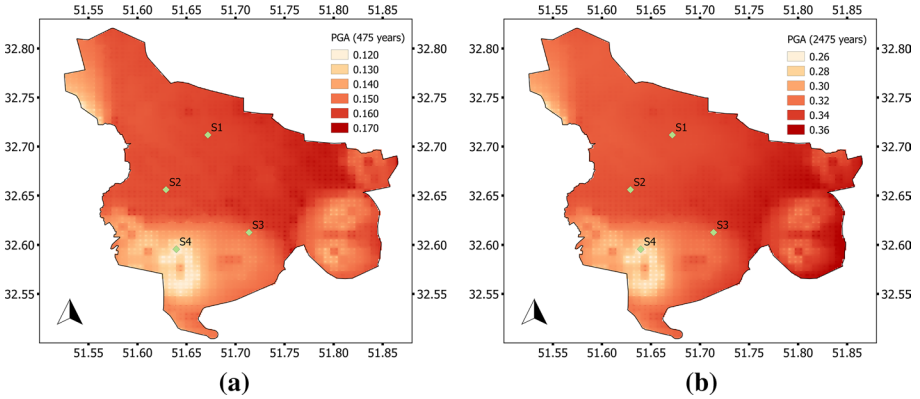

Fig. 3 Isfahan *PGA* hazard maps based on the EMME source model for: **a** 475-year return period; **b** 2475-year return period. Four representative sites (S1–S4) are indicated

properties. Discussions about different approaches to compute the site amplification factors can be found in Sandıkkaya et al. (2018). These more refined methods, however are not applicable in studies involving thousands of sites, such as the one presented here.

3.4 Probabilistic seismic hazard analysis results

The OpenQuake engine (Silva et al. 2014) is used here for computing the seismic hazard curves and maps. This platform has been developed within the Global Earthquake Model (GEM) initiative for seismic hazard and risk computations. We performed PSHA using the EMME source model for more than 28,500 grid points spatially distributed at a 0.0014×0.0014 decimal degrees resolution (about 15.0 m) to show the variation of the seismic hazard across Isfahan. For the purposes of this section, we computed the hazard curves at each grid point and, from them, we extracted the hazard maps for 2% and 10% in 50 years probability of exceedance (i.e., return periods of 2475 and 475 years, respectively). These results include hazard curves for different *IM*s, such as *PGA* and *Sa*(*T*), computed for each branch of the source model and GMPE logic trees. Figure 3 shows the *PGA* hazard maps for return periods of 475 and 2475 years, while Fig. 4a displays the histogram of *PGA* values computed for all the grid points both extracted from the mean hazard curves. For 475 years, the *PGA* ranges from 0.12 to 0.18 g with an average value of 0.15 g, while for 2475 years it ranges from 0.25 to 0.37 g with an average value of 0.33 g. The trends of *PGA* estimates obtained here are spatially in agreement with those from a previous study (Tajmir Riahi et al. 2014) performed for supporting the seismic zonation of Isfahan: in both studies the larger intensities are observed in the central to northern regions while lower intensities are estimated in the south. Although the spatial pattern is the same, there is a disagreement in terms of intensity as Tajmir Riahi et al. (2014) estimated *PGA* values on rock ranging between 0.125 and 0.265 g for 475 year return period, values that are further amplified when accounting for the soil effects. Part of this inconsistency may be related to the differences in the seismogenic sources and in the different GMPEs considered in the two studies. Another aspect contributing to this discrepancy may be the software adopted for the computation of the hazard in the two studies (Kohrangi et al. 2018).

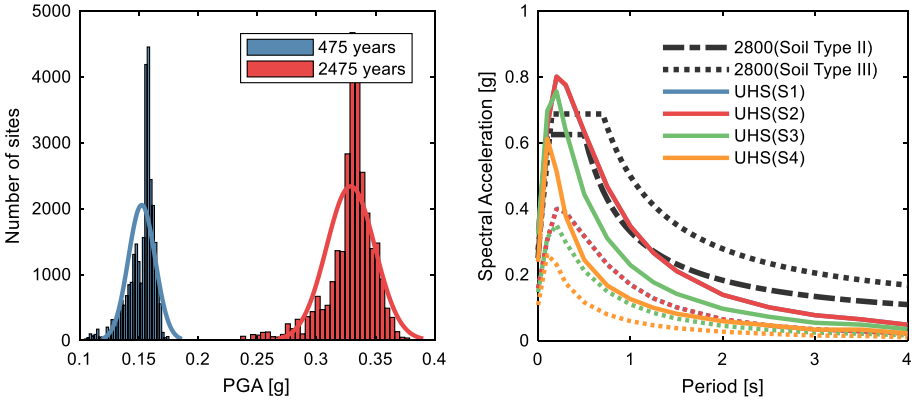

Fig. 4 **a** Histogram of *PGA* values for return periods of 475 and 2475 years estimated at all the 28,500 grid points where hazard curves are computed; **b** comparison between the Uniform Hazard Spectrum (UHS) obtained from the EMME hazard source model at four different sites (i.e., S1–S4 in Fig. 3) and the design spectrum for soil types II and III based on Standard 2800 (version IV) for Isfahan. The dotted colored lines represent the 475-year return period UHS and the colored solid lines refer to the 2475-year return period UHS

Figure 4b compares the uniform hazard spectra (UHS) for 475- and 2475-year return periods at the four individual sites named S1, S2, S3 and S4 in Fig. 3, where the Vs_{30} estimates are 224, 223, 388 and 730 m/s, respectively. Based on these values, S1 and S2 correspond to soil type III, while S3 and S4 correspond to soil type II according to Standard 2800. Figure 4b also shows the design spectrum proposed by Standard 2800 for sites located on soil type II and III. As can be seen, the 475-year UHS estimates are almost half of those of the design spectrum. Based on this preliminary result, one should expect considerable added safety for the buildings designed according to Standard 2800, simply because it prescribes highly conservative design loads. This comment will be re-visited and further elaborated on in the following section when the results of building seismic risk assessment are presented.

4 Exposure, fragility and vulnerability modeling

Isfahan consists of 15 municipal districts that are distributed in a land area of about 551 km^2. According to the 2011 Census data, there are more than 15,600 city blocks in Isfahan with about 485,000 individual buildings and about two million inhabitants. The companion paper (Kohrangi et al. 2021) discussed the procedures used for generating the building taxonomy and the exposure model, and the derivation of fragility and vulnerability curves for Isfahan. Therein, we identified 27 building classes based on the material type (i.e., Adobe, unreinforced Masonry, infilled Reinforced Concrete, and steel), age (i.e., "No-Code", "Mid-Code" and "High-Code" labeled as "NC", "LC" and "HC", respectively) and height (i.e., "Low-rise", "Mid-rise" and "High-rise", or "LR", "MR" and "HR", respectively). In addition, we considered several building sub-classes that account for the lateral load resisting systems. Table 1 shows a list of the building classes and their acronyms together with the building counts and the total number of residents in each building class. According to

Table 1 List of the building counts and the total percentage of city residents for each building vulnerability class specified by the adopted exposure model

Number	Class Description	Acronym	Building count (%)	Population (%)
1	Adobe	Adobe	4.02	2.27
2	Unreinforced Masonry, Low-Rise	URM-LR	36.69	26.90
3	Unreinforced Masonry, Mid-Rise	URM-MR	1.64	2.85
4	Steel Moment frame, No-Code, Low-Rise	SMF-NC-LR	0.47	0.31
5	Steel Moment frame, Mid-Code, Low-Rise	SMF-MC-LR	1.16	0.75
6	Steel Moment frame, High-Code, Low-Rise	SMF-HC-LR	8.99	6.38
7	Steel Moment frame, No-Code, Mid-Rise	SMF-NC-MR	0.37	0.61
8	Steel Moment frame, Mid-Code, Mid-Rise	SMF-MC-MR	0.89	1.39
9	Steel Moment frame, High-Code, Mid-Rise	SMF-HC-MR	6.34	10.70
10	Steel Moment frame, No-Code, High-Rise	SMF-NC-HR	0.00	0.00
11	Steel Moment frame, Mid-Code, High-Rise	SMF-MC-HR	0.06	0.09
12	Steel Moment frame, High-Code, High-Rise	SMF-HC-HR	0.31	0.50
13	Steel braced frame, Low-Rise	SBF-MC-LR	1.16	0.75
14	Steel braced frame, Mid-Rise	SBF-MC-MR	0.89	1.39
15	Steel braced frame, High-Rise	SBF-MC-HR	0.06	0.09
16	RC Infilled frame, No-Code, Low-Rise	RCF-NC-LR	0.76	0.50
17	RC Infilled frame, Mid-Code, Low-Rise	RCF-MC-LR	2.96	1.93
18	RC Infilled frame, High-Code, Low-Rise	RCF-HC-LR	16.68	11.90
19	RC Infilled frame, No-Code, Mid-Rise	RCF-NC-MR	0.60	1.08
20	RC Infilled frame, Mid-Code, Mid-Rise	RCF-MC-MR	1.18	2.04
21	RC Infilled frame, High-Code, Mid-Rise	RCF-HC-MR	5.87	10.57
22	RC Infilled frame, Mid-Code, High-Rise	RCF-MC-HR	0.12	0.33
23	RC Infilled frame, High-Code, High-Rise	RCF-HC-HR	0.80	1.84
24	RC dual frame-wall, Mid-Code, Mid-Rise	RCWF-MC-MR	1.18	2.04
25	RC dual frame-wall, High-Code, Mid-Rise	RCWF-HC-MR	5.87	10.57
26	RC dual frame-wall, Mid-Code, High-Rise	RCWF-MC-HR	0.12	0.33
27	RC dual frame-wall, High-Code, High-Rise	RCWF-HC-HR	0.80	1.84

this Table, "URM-LR" and "RCF-HC-LR" with about 37% and 17%, respectively, are the most adopted building classes while most of the population of the city reside in the "URM-LR" (27% of the population), "SMF-HC-MR" (11%), "RCF-HC-LR" (12%), "RCF-HC-MR" (11%) and "RCWF-HC-MR" (11%) building classes.

For each building class we computed sets of class- and region-specific fragility and vulnerability curves based on nonlinear response time-history analysis of equivalent single-degree-of-freedom systems that account for both building-to-building and record-to-record variability. We considered the four different damage states of "Slight", "Moderate", "Extensive" and "Collapse" to develop the fragility curves. Subsequently, they were combined with a consequence model to obtain vulnerability curves. A consequence model provides the distribution of repair cost associated with fixing (or replacing) a building in any given damage state to its pre-earthquake conditions, normalized by the building total replacement cost. In our consequence model, we used average loss ratios equal to 0.1, 0.3, 0.6 and 1.0 for slight, moderate, extensive and collapse damage

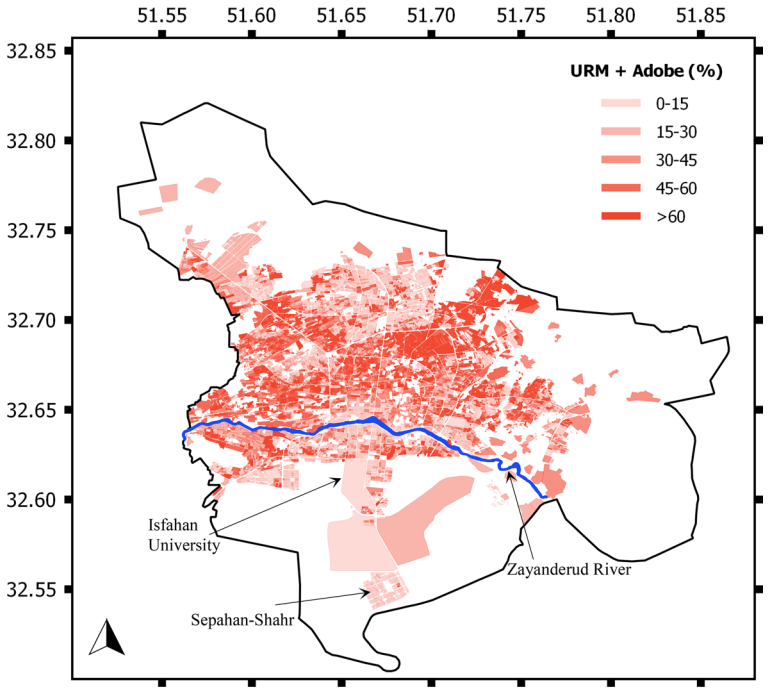

Fig. 5 Spatial distribution of the "URM" (both LR and MR) + "Adobe" building classes in terms of percentage to the total number of buildings at individual blocks

states, respectively. The adopted fragility and vulnerability curves employ one of the spectral accelerations at 0.2, 0.3, 0.5, 0.7 and 1.0 s as ground motion *IM* depending on the fundamental period of each building class. The exposure model was created at the city block level to define the spatial distribution of the building classes as well as the population in the area of interest. More details on the exposure, fragility and vulnerability modeling of this study are provided in the companion paper (Kohrangi et al. 2021). As an example, Fig. 5 shows a map of the spatial distribution for the aggregated "URM-LR", "URM-MR" and "Adobe" building classes that jointly comprise about 44.3% of all buildings in Isfahan (Table 1). These are the oldest and most seismically vulnerable classes and their distribution approximately maps the age of buildings in Isfahan.

Referring to Fig. 5, these buildings are prevalent (shown in dark red color) in the northeastern parts of Isfahan mainly north of the Zayanderud River where the oldest historical core of the city is located. More recent urban expansions can be found in the northern wedge and south of the river (blocks shown in light red on Fig. 5) where more recent steel and RC constructions are dominant. As an example, Sepahan-Shahr (shown on the map of Fig. 5) is a small residential area in south-west of Isfahan established in 1992. This area was planned to host a part of the residents of Isfahan to reduce the compact population of the city. Its construction started around 1996, which is approximately in the transition interval from the "Mid Code" to "High Code" eras. Most of the buildings in Sepahan-Shahr are residential RC apartments with mainly 2–6 number of stories. As such, the most prevalent building classes in this area are "RCF-MC-LR" (15% of all buildings), "RCF-HC-LR" (24%), "RCF-MC-MR" (20%) and "RCF-HC-MR" (32%).

5 Seismic risk assessment

We employ the exposure model, the fragility and vulnerability functions of Kohrangi et al. (2021) as described above to perform (1) seismic damage assessment and (2) loss estimation for the building stock and population of Isfahan. Damage assessment basically quantifies the percentage of buildings that after the occurrence of an earthquake may transition from a "No damage" state to one of the four damage states ranging from "Slight" damage to "Collapse". In this type of analysis, the fragility curves are utilized to evaluate the probability that any given building belonging to a given class located at a given site may end up in any one of the damage states when subject to any given level of ground motion *IM*. Loss estimation instead evaluates the distribution of direct losses (e.g., monetary losses or human injuries) to repair or replace damaged buildings. For this second purpose, we utilize vulnerability curves. Damage assessment and loss estimation can be performed probabilistically for one scenario only (i.e., *scenario-based* assessment), or for multiple scenarios (i.e., *time-based* assessment). This terminology is adopted from FEMA-P58 (2012), where the interested reader can find more details about each approach. Nevertheless, herein to help the readers better understand the features and application of each method in the portfolio seismic risk assessment, we provide brief descriptions in the following sub-sections.

5.1 Scenario-based damage and loss assessment

Scenario-specific results are easier to grasp even by less sophisticated stakeholders and are almost always included in risk assessment studies despite being of rather limited value for decision making. It is very common to consider scenarios to help better understand the probabilistic results of the time-based assessment studies discussed later. For example, a loss of a certain amount that has, say, a 10% chance in 50 years of been reached or exceeded is more readily assimilated and understood by most stakeholders if the analyst chooses an appropriate scenario, say M7.0 event at 30 km, that is likely to cause it. The correspondence of probabilistic loss results and scenario-based losses also helps communicating risk to the public at large. The outputs of a scenario-based assessment are essential for emergency management and natural hazard mitigation programs (ATC20 1989; Whitehead and Rose 2009) in an urban area, or for individual as well as societal and environmental risk management (Jonkman et al. 2003). The spatial distribution of the damages and the level of damage (usually graded based on "green, "yellow" and "red" tagging per ATC 20 (1989) can form the basis for a comprehensive post-disaster emergency planning or to design risk mitigation strategies. Moreover, the scenario-based outputs facilitate rapid and effective economic and human loss estimation, which is of utmost importance in the immediate aftermath of earthquake disasters (Erdik et al. 2011; Jaiswal and Wald 2013).

Technically, the main objective of a scenario-based assessment is to estimate the distribution of the portfolio loss caused by the considered earthquake. The portfolio loss is a random variable (RV), which is the sum of the losses experienced by the n buildings in the portfolio, where n here is the number of buildings at all the grid points in Isfahan. The distribution of the sum of n random variables, which can be many hundreds of thousands in a portfolio loss analysis, can be computed using an operation called convolution (Benjamin and Cornell 1970). Performing convolution is computationally straightforward when the RVs are independent. The main complication here is that the n random variables corresponding to the losses of all buildings in a portfolio are

dependent and their covariance structure is complex. This dependence comes from two sources. Firstly, the ground motion *IM*s caused by the same earthquake at any building location are correlated random variables and their degree of correlation decreases with increasing distance between the sites. This correlation has been estimated empirically from ground motion recordings of past events such as Baker and Jayaram (2008). Hence, the losses at different buildings, which are functionally dependent on these *IM*s via the vulnerability functions, are themselves also statistically dependent RVs in a way that decreases with increasing distance between building sites. Secondly, the losses of two different buildings belonging to the same construction class (say, reinforced concrete frame, mid-rise, of the 1980s) are also dependent because the vulnerability function utilized for estimating their losses given *IM* may be biased. The bias may stem from our partial knowledge of how the buildings belonging to a class may respond to earthquakes. They may all respond better or worse than what one anticipates when developing the corresponding vulnerability function based on engineering principles and, sometimes, few empirical observations. This is especially true for recent buildings that have not been tested yet by any severe earthquake. This second source of correlation is very difficult to quantify (Bazzurro and Luco 2005, 2007; Silva 2019) and in practical applications it is either neglected or, assumed to be described (for all buildings in a class regardless of their geographical spacing) by a constant correlation coefficient usually ranging from 0.2 to 0.4.

The convolution of many thousands of dependent RVs with this complicated covariance structure is an intractable mathematical problem that cannot be solved in closed form. To circumvent this complication, for computational expediency the portfolio loss distribution caused by an earthquake is estimated here via Monte Carlo simulation. In this simulation we account for the first and most critical source of correlation for regional and urban risk assessment studies (Goda and Hong 2008; Park et al. 2007; Weatherill et al. 2015) and, given the lack of supporting data, we disregard the second, less important one. Neglecting completely these two sources of correlation would lead to a significant underestimation of the likelihood of observing very high losses (and, less importantly, very low losses) that earthquakes may cause. Hence, for each selected scenario we use OpenQuake to simulate multiple random fields of the vector of ground motion *IM*s of interest based on a given GMPE (see Sect. 3.2 for those utilized here). These random fields are probabilistic representation of the ground motion *IM*s that the selected earthquake may generate in the affected region. In each random field, the values of these *IM*s at any grid point are then used to probabilistically evaluate the losses for each building class located there (see Fig. 5 for adobe and URMs). As explained above, for each earthquake these random fields contain *IM*s that are correlated at any pair of sites as follows: same *IM*, e.g., $Sa(T_1)$ values at site 1 and site 2 in a way that decreases with increasing site-to-site distance; different *IM*s at the same site, e.g., $Sa(T_1)$ and $Sa(T_2)$, in a way that decreases with the difference between periods T_1 and T_2. Note that the relatively weaker spatial cross correlation among different *IM*s at different sites, e.g., $Sa(T_1)$ at site 1 and $Sa(T_2)$ at site 2, is not modeled here.

The results of the scenario-based analyses are usually expressed in terms of the probabilistic distributions of the quantities of interest, such as monetary losses, human losses, buildings collapsed, non-serviceable buildings, and number of displaced (or homeless) people, and their summary statistics (e.g., mean, median and other quantiles). Of course, these distributions are conditional on the occurrence of the scenario earthquake, the likelihood of which in a given period of time is not provided by the scenario-based analysis.

5.2 Time-based risk assessment

Time-based risk assessment is simply performed by repeating the scenario-based analysis discussed above for "all" foreseeable earthquakes that may affect the region of interest in the future and then weigh the distributions of the resulting quantities, namely damage and losses, computed for each earthquake by its likelihood of occurrence in the time period of interest (say 1 year or 50 years). As alluded to earlier, the more comprehensive results of time-based risk assessment have naturally a wider range of applicability than scenario-based ones, especially in decision making and the insurance industry (Goda 2015; Goda et al. 2014; Goda and Yoshikawa 2012; Zhao et al. 2019). Even though the present study mainly focuses on monetary and human life losses, the procedure described here holds also for any other quantity of interest such as the ones mentioned earlier (e.g., downtime, displaced people). Note that here we utilize the time-based assessment approach for two different purposes. Firstly, to estimate the losses *separately for each building* of the construction classes that exist at any specific grid point in Isfahan. In other words, these are not portfolio loss results of the ensemble of all buildings in Isfahan but rather a collection of many thousands of single-site building-specific loss estimation studies, meaningful when considering each property separately, e.g., as an individual owner. Secondly, to evaluate the likelihood of different amounts of losses that *the entire building exposure* in the city, considered as a single portfolio, can experience, thus adopting the view of regional or municipal administration, or an insurer who has underwritten the policies for the entire area.

The former set *building-specific loss* results are customarily expressed in terms of the so-called loss exceedance curves, any value of which is associated to a loss that is expected to be reached or exceeded, with a given probability in a given time period (e.g., 1% per year), or, alternatively, on average once every certain number of years (e.g., 100 years), called return period. Will discuss later how these curves can be computed. These losses are the direct costs for fixing the specific building to its pre-earthquake conditions. Strictly speaking each of these loss exceedance curves is a complementary cumulative distribution function of the losses generated for the specific building by all events multiplied by the probability that any earthquake of magnitude above the minimum value considered in the analysis (usually M4 to M5, depending on the vulnerability of the building stock in the study region; here we used M4.5) occurs in the period of interest (e.g., 1 year or 50 years). The availability of these curves for all buildings across the city allows us to generate two sets of loss results. The first is a set of maps showing the spatial distribution and magnitude of losses that can occur with a given likelihood per year to buildings of different classes across the city (see Figs. 8 and 9 to come). The second set of results will show the average annual losses (AALs), which are the losses that the buildings of different classes are expected to withstand, on average, every year due to earthquakes over a long period of time (see Fig. 11 to come).

The latter set of *portfolio* loss results are also customarily expressed in terms of the loss exceedance curves, but this time the losses refer to the portfolio as a whole, which here is the entire building stock in Isfahan. As discussed in the scenario-based analysis, for each earthquake the portfolio loss is simply the sum of the losses experienced by each building in the portfolio. The AAL for the entire building stock is equal to the sum of the AALs of all the buildings in it. It is interesting to note, however, that the associative property does not apply to exceedance probability curves. In simple words, the exceedance probability curve even for the simplest possible portfolio, namely one

that include any pair of buildings in Isfahan, is not equal to the sum of the exceedance probability curves of the two buildings. Therefore, the exceedance probability curves of Building 1, that of Building 2, and that of the portfolio comprising both buildings need to be computed using three separate sets of computations.

As mentioned earlier, the computation of the exceedance probability curves for either the entire portfolio of buildings or a single building is done by weighing the distribution of losses for any considered earthquake (as done in the scenario-based analysis) by its likelihood of occurrence in the period of interest. The exceedance probability curve for any building at a specific location can, in fact, be computed exactly in the same fashion as done for a portfolio. Namely, for each earthquake one could extract from each realization of the random fields the value of the *IM* of interest at the specific site and using it to estimate the losses for that building for that realization. Repeating the same exercise for all the realizations of the random fields would deliver an estimate of the loss distribution for that building for that earthquake. The distribution of the losses for each earthquake are then weighed as stated above. This approach, however, leads to accurate results for single buildings only if one performs many realizations of random fields for each earthquake. This would be an exceptionally time-consuming task, which is usually avoided in favor of numerical integration, which is the approach adopted here. Numerical integration, unfortunately, is not feasible for computing portfolio losses because of the dependence among losses for different buildings discussed above. The numerical integration framework is essentially identical to that adopted in classical PSHA. For each event, the distribution of the ground motion *IM* at each building site (from PSHA) is convolved with the vulnerability curve of the building to obtain the building loss distribution for that earthquake. This operation is repeated for all earthquakes and the distribution of building losses is obtained by weighing each earthquake-specific building loss distribution by its probability (or rate) of occurrence in the period of interest.

6 Risk analysis results and discussion

6.1 Scenario-based damage and loss estimates

As an example, we consider two earthquakes: M5.5 and M6.5 with epicenters at (51.846°E, 32.727°N) and (52.260°E, 32.998°N) located north east of Isfahan about 10 and 60 km away from the center of the city, respectively, at a depths of 5 and 10 km. The location of the hypothetical epicenters is shown in Fig. 6a. As will be shown later, these are two likely scenarios to cause aggregated losses exceeding the 100-year return period loss for the entire building portfolio. Figure 6b shows the percentage of the expected collapsed buildings at the block level for the M5.5 earthquake, while Fig. 6c illustrates, for both the M5.5 and M6.5 scenarios, the percentages of all buildings in the entire city that are expected to experience "No Damage", "Slight", "Moderate", "Extensive" and "Collapse" damage levels. For instance, for the M6.5 earthquake about 52% of the expected buildings are expected to experience no damage while for M5.5 this number is 58%. On the other hand, 8% to 9% of the buildings are expected to collapse in both scenarios.

Figure 7 shows the distribution of the aggregated losses for the entire city in terms of the monetary losses and the number fatalities expected for the M5.5 and M6.5 earthquake scenarios. The expected monetary losses induced to all the buildings in Isfahan are estimated to be equal to 1.95 and 2.20 billion € for the M5.5 and M6.5 earthquake scenarios,

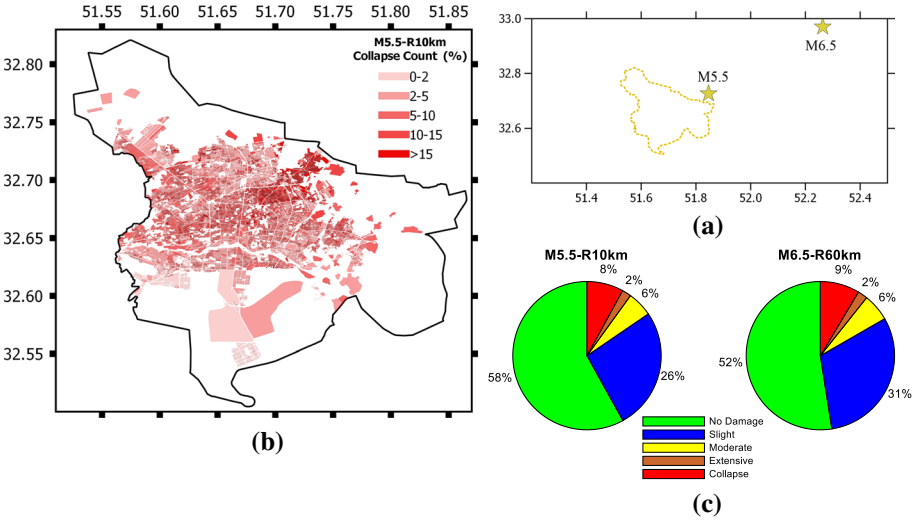

Fig. 6 **a** Location of the hypothetical epicenters; **b** spatial distribution of the expected building counts (in percentage) at the block level that are expected to experience the "Collapse" limit state for the M5.5 earthquake; **c** Pie charts showing the expected percentage of buildings in the different damage states of "No Damage", "Slight", "Moderate", "Extensive" and "Collapse" after the M5.5-R10km and M6.5-R60km earthquakes

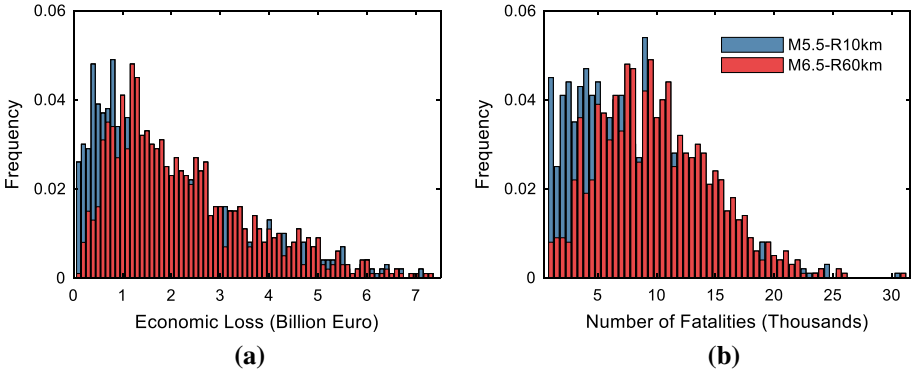

Fig. 7 Distribution of the scenario-based economic losses (**a**) and human losses (**b**) caused by the M5.5 and M6.5 earthquakes

respectively. The disaggregation of the estimated monetary loss contribution in terms of material, age and height for the M6.5 earthquake scenario shows that about 80% of the induced monetary losses are due to the "URM" and "Adobe" building classes, which besides being the most prevalent building classes in Isfahan, they are more seismically vulnerable than all the code-designed buildings (see fragility and vulnerability curves discussed in the companion paper, (Kohrangi et al. 2021). Overall, the "No-Code" building classes are the cause for 82% of the monetary losses, while the loss due to "Low-rise" buildings is about 83% of the total. The estimated number of fatalities (i.e., the I_5 injury

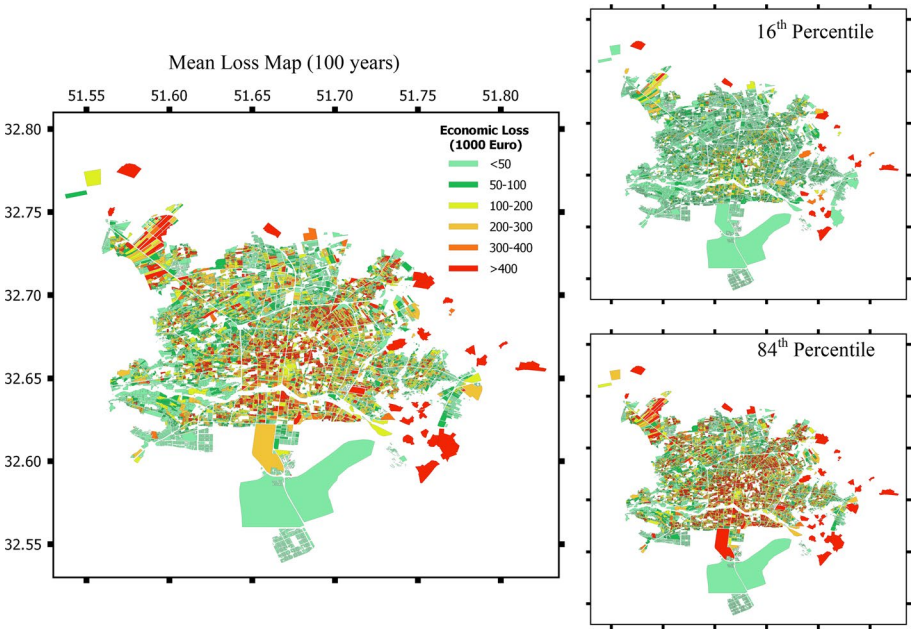

Fig. 8 Mean, 16th and 84th percentiles economic loss (aggregated at the block level) maps for Isfahan corresponding to a probability of exceedance of 39% in 50 years (100-year return period)

type denoted in Table 4 of the companion paper (Kohrangi et al. 2021)) are 7750 and 9920 for the M5.5 and M6.5 earthquakes, respectively, if they occur during night time when we assume that 95% of the people are indoors in their residential dwellings. It should be noted that based on our assumptions, fatalities only occur when a building enters Collapse, about 81% of which are "URM" and "Adobe" for the M6.5 scenario.

6.2 Time-based damage and loss estimates

In this section we present the results obtained from the risk-based assessment. Note that in our computations we generated single catalog of simulated earthquakes with 10,000 realizations of next year's seismicity. Figure 8 shows the economic loss maps for the entire city that display the *building-specific losses* corresponding to 39% probability of exceedance in 50 years (100-year return period). In this figure, besides a map with the mean losses, we also show the maps with the 16th and 84th percentiles of the monetary losses that quantify the uncertainty in these estimates. Different colors shown on the map represent different aggregated loss values for each block of the city. To avoid misinterpretations, one should realize that the number of buildings and, therefore, the total replacement cost vary considerably by block. Therefore, in Fig. 9 we show again the maps of mean losses by block for the 39% and 10% probabilities of exceedance in 50 years (i.e., 100 and 475 year return periods, respectively) but this time normalized (shown in percentage) by the total replacement cost of all buildings within the block. It should be noted that the variations in the loss estimates (e.g., the 16th and 84th percentiles) reported herein are only due to the variations in the epistemic uncertainty considered in the ground motion source modelling and the

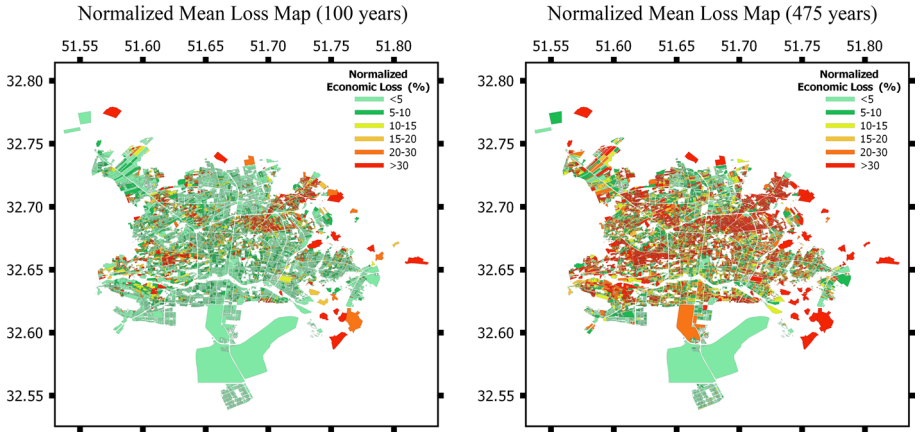

Fig. 9 Mean economic loss maps (aggregated at the block level and normalized to the total replacement cost of each block) for Isfahan corresponding to a probability of exceedance of 39% in 50 years (i.e., 100-year return period) and 10% in 50 years (i.e., 475 years return period)

epistemic as well as aleatory uncertainty in the ground motion intensity. Other sources of uncertainty (e.g., in the exposure model) are not considered in this study.

Comparing Fig. 8 with Fig. 5, which shows the spatial distribution of the "URM" and "Adobe" building classes, one may generally observe a similar trend. This is a visual confirmation of what was stated earlier for the scenario events, namely that a large part of the losses is caused by the "URM" and "Adobe" buildings, which are highly vulnerable and more prevalent compared to other building classes in many areas of Isfahan. Conversely, there are also some areas in the south that do not follow the trends of Fig. 5 and show "unexpected" large seismic losses. These parts are mainly populated by mid-code and high-code buildings that are expected to be less vulnerable but still show high loss values. This is because in those areas most of the buildings are mid-rise and high-rise (i.e., buildings with more than 3 stories), which naturally increase the exposure at risk. This apparent anomaly disappears when one scrutinizes Fig. 9, where the normalized losses in the southern part rarely exceeds 10% of the total replacement cost. On the other hand, in the north-eastern parts that host many "URM" and "Adobe" buildings (see Fig. 5), there are numerous blocks with normalized losses exceeding 30%.

Figure 10 shows the aggregated loss exceedance curves for *the entire building exposure* in terms of both monetary losses and human losses. The 50th/16th/84th percentiles aggregated economic losses (and fatalities) for the 100-year return period are estimated as 1.27, 0.71, and 1.50 billion Euros (5800, 3700 and 7000 deaths), respectively. For the 475-year return period these estimates increase to 3.74, 2.74, and 4.35 billion Euro (15,600, 12,400, and 19,100 deaths), respectively. We emphasize again that these estimates refer to direct losses due to structural and non-structural damage only and consider neither building contents losses, nor indirect losses due to business interruption. The total AAL caused by earthquakes for the entire building stock in Isfahan is about 43.1 million Euro, which corresponds to about 1.9‰ of the total replacement cost of the inventory (namely 26.21 billion Euro). Figure 11a shows the absolute values of the average annual losses (AAL) per building class while Fig. 11b displays the same AAL values by class by but normalized by the total replacement cost of the class. As expected, the highest normalized AAL values are those of "Adobe" buildings (about 7.5‰) and of "URM" buildings (about 5‰).

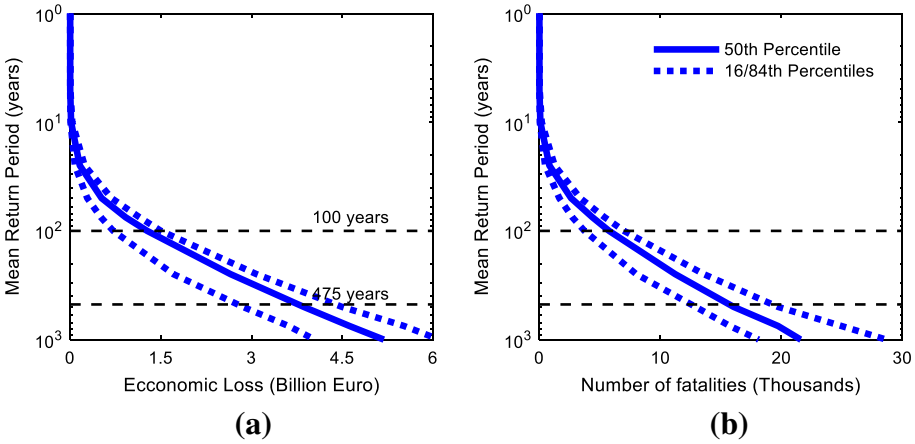

Fig. 10: 16th/50th/84th percentiles of the aggregated loss exceedance curves for the entire building stock of Isfahan: **a** direct economic losses to buildings (no contents); **b** number of fatalities

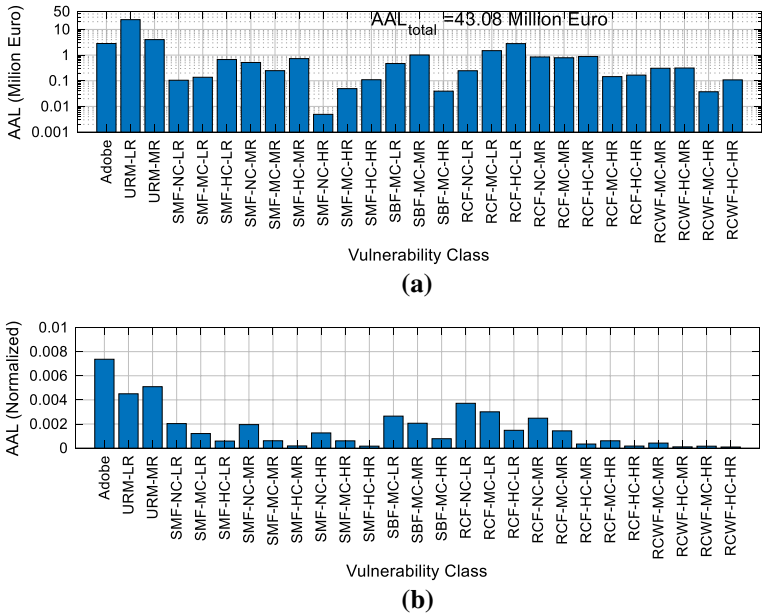

Fig. 11 Average annual loss (AAL) induced by earthquakes to the 27 different classes of buildings in Isfahan: **a** absolute values; **b** values normalized by the total replacement cost of the class

Noteworthy, are also the losses in older, pre-code RC frame buildings with AAL values of about 3–4‰.

Figure 12, which provides a distillation of Fig. 11, shows the contributions of the buildings in different bins of material vs. height and material vs. construction year to the total AAL of the entire building inventory in Isfahan. This Figure, for example, further emphasizes that almost 50% of the AAL in the entire city is due to the losses to the (no-code)

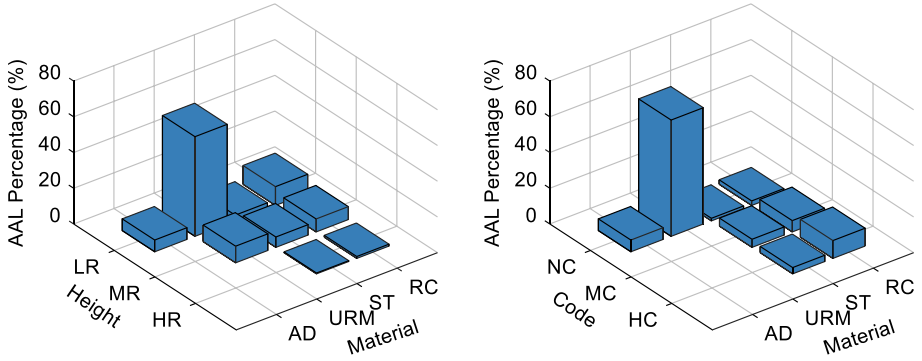

Fig. 12 Economic loss by construction material, height and age for a probability of exceedance of 10% in 50 years (return period of 100 years). Legend: *HC* high code, *MC* mid code, *LC* low code, *HR* high rise, *MR* mid rise, *LR* low rise, *AD* Adobe, *URM* unreinforced masonry, *ST* steel, *RC* reinforced concrete (both frames and dual)

"URM" buildings, which are not engineered for seismic loads. It should be noted, however, that the recent Kerman-Shah 2017 earthquake (Alavi et al. 2018) has showed also unexpectedly high levels of damage in engineered Iranian buildings, such as steel and reinforced concrete buildings, that were mainly due to poor construction practices employed not allowed by the building code in force. In our analysis, however, we decided not to include this detrimental human factor into the development of vulnerability functions of engineered buildings assuming that Isfahan has a tighter government oversight enforcing code compliance, as usually happens in larger cities and closer to the capital. Thus, one may expect lower losses in Isfahan due to seismically designed buildings. Yet, it is interesting to note that "RCF-HC" classes seem to contribute to the absolute losses slightly more than the "RCF-NC" classes. The reason is simply the scarcity of "No Code" RC buildings (with 2 or fewer stories) compared to the Low-rise and Mid-rise "Mid-Code" and "High-Code" RC buildings (see Fig. 4 of the companion paper) in the exposure inventory resulting in their lower aggregated monetary values.

7 Concluding remarks

A seismic risk assessment study was presented for the building inventory of the historical city of Isfahan, Iran. It utilizes a state-of-the-art probabilistic approach and is underpinned by a very detailed exposure database of residential, mixed residential/commercial, and public buildings, which is uncommon in urban-scale studies. Several are the observations and lessons learned:

- First and foremost, it is a difficult and time-consuming task to gather and interpret all the different datasets needed for a detailed urban-scale risk assessment study. The co-operation with local authorities and researchers is critical, not just for data gathering but also for data interpretation, especially about construction practices, code enforcement and damage patterns expected for each building class.
- Empirical damage/loss data to develop fragility/vulnerability functions are seldom available, especially for cities in the Middle East. Hence, a code-compatible system

"design" approach that divides the entire building stock into classes of like buildings supported by analytically derived vulnerability curves is the best viable option left to the analyst. However, to ensure realistic vulnerability assessment, extreme care needs to be taken in using ground motion records as input to the nonlinear dynamic analysis, selecting them to be consistent with the local hazard, as done here.

- The seismic hazard characterization is key, while epistemic uncertainty in earthquake recurrence and ground motion prediction should always be modeled. In addition, resources permitting, a geological investigation of the faults that may be located close to the city should be carried out. In our study we relied on the best regional earthquake hazard model available, but we did not perform any local in situ geological investigation.
- Soil site characterization via a topographical slope-based approach quickly resolves a big hole of in missing geotechnical data and is usually adopted in most regional and urban level studies. However, the accuracy of Vs_{30} estimates should always be tested to avoid gross errors in site amplification. In our study, in general we found a good agreement between V_{S30} estimates based on borehole tests and those based on topography that were utilized in the risk computations.
- Adobe and unreinforced masonry buildings are the most vulnerable assets of any old city, and Isfahan is no exception. In this case they contribute the majority of economic loss, injuries and fatalities and have AAL values ranging from about 5.4–7.5‰. Older RC frames are the second largest contributors with AALs between 3.4 and 4.4‰.
- The total AAL for Isfahan is about 43 million Euro, which corresponds to about 1.9‰ of the total replacement cost of the inventory.
- On average once every 100 years Isfahan can expect losses in the order of 1.3 billion euros in direct building losses (no contents included) and about 4000 fatalities caused by earthquakes.

The economic and human loss estimates for the entire building inventory computed here can be used to improve the resilience of Isfahan to future earthquakes. For example, these estimates are critical for devising risk mitigation strategies that are targeted to save lives and reduce the economic impact of earthquakes that surely will affect Isfahan in the future. Retrofitting measures (including in some cases replacement) can be tailored for the most vulnerable buildings and for those that are most critical to the normal operations of the city (public buildings, police stations, firefighters' stations, hospitals, and schools). Information about human casualties after future earthquakes can be used, for example, for testing the capacity of the local health system (i.e., hospitals and clinics) to receive a sudden large influx of injured victims after an event. Risk mitigation strategies may also include acquiring earthquake insurance coverage without which the economy after earthquakes in many parts of the world has shown not to fully recover for many years. The economic losses by building class here can provide unbiased estimates of pure premiums for insurance policies.

It should be noted that, in any portfolio loss assessment study, a validation of the final loss estimates is always advisable. We could not find any available data for the region of Isfahan, however, to do so. Nevertheless, we informally carried out several checks that were based on AAL estimates only and they are not reported in the paper. The AALs presented here were compared with those of similar buildings in other moderately hazardous areas of the world. The reason for not showing these comparisons is that those AALs, which we used to convince ourselves of the legitimacy of the numbers we presented, are not in the public domain but are rather provided by proprietary catastrophe risk models used in the insurance industry. Although it would make the paper stronger, we cannot show them here.

Overall, the results are indicative of what one should expect from any major urban area of the Middle East in a moderately seismic hazard setting. The risk estimates provided here are robust but, nonetheless, can be improved in several ways, for example by enhancing the nearby fault modeling via in-situ geologic investigations and the soil characterization by gathering all the geotechnical tests performed for permitting of important buildings in the city. Also, the loss estimates computed should be augmented with building content losses, neglected here, and with infrastructure losses, without which a comprehensive resilience plan for a city cannot be devised. Finally, the historical core of Isfahan is a UNESCO World Heritage site comprising multiple unique buildings that require targeted studies to more accurately estimate their seismic risk, to gauge the impact of their loss on the city's and the citizens' financial livelihood, and to design specific risk mitigation measures.

Acknowledgements The authors wish to acknowledge the technical support of Dr. Laurentiu Danciu in the selection of GMPEs and the application of the EMME source model. We would also like to thank Dr. Bahram Nadi for his suggestions on the spatial distribution of different soil types in Isfahan. We thank Dr. Fabrizio Pelli for useful discussions in interpreting the geotechnical experimental test results. We are grateful to Mauro Mangini, Dr. Ettore Fagà and Anna Mottadelli of RED for their help with GIS technical suggestions and providing the computational resources to perform the hazard and risk analyses of this study. We are also grateful for the technical comments about OpenQuake modeling provided by Dr. Vitor Silva and Dr. Michele Simionato at GEM foundation. We thank the Isfahan Urban Railway Organization for providing us with the geotechnical reports for Isfahan. Finally, we thank the associate editor and three anonymous reviewers whose comments and suggestions significantly increased the quality and the clarity of this manuscript.

Funding The first author is grateful for the financial support provided by the Iranian National Elites Foundation and by the Scuola Universitaria Superiore IUSS Pavia. Additional financial support has been provided by the Executive Agency for Small and Medium-sized Enterprises (EASME) under the powers delegated by the European Commission through the Horizon 2020 program "HYPERION- Development of a decision support system for improved resilience & sustainable reconstruction of historic areas to cope with climate change & extreme events based on novel sensors and modelling tools", Grant Agreement Number 821054.

Compliance with ethical standards

Conflict of interest The authors declare that they have no conflict of interest.

References

Abdi F, Mirzaei N, Shabani E (2013) Ground-motion scenarios consistent with PSH deaggregation for Tehran, capital city of Iran. Nat Hazards Earth Syst Sci 13:679–688. https://doi.org/10.5194/nhess-13-679-2013

Abdolahi M, Jafarian M, Goodarzi G, Pirhadi G, Partoazar H (2014) Geology map reports for Isfahan-Felavarjan. Geological Survey & Mineral Explorations of Iran (GSI), Zamin danesh Pars Engineering consultants, Tehran

Abrahamson N, Silva W (2008) Summary of the Abrahamson & Silva NGA ground-motion relations. Earthq Spectra 24:67–97. https://doi.org/10.1193/1.2924360

Abrahamson NA, Silva WJ, Kamai R (2014) Summary of the ASK14 ground motion relation for active crustal regions. Earthq Spectra 30:1025–1055. https://doi.org/10.1193/070913eqs198m

Akkar S, Cagnan Z (2010) A local ground-motion predictive model for Turkey, and its comparison with other regional and global ground-motion models. Bull Seismol Soc Am 100:2978–2995. https://doi.org/10.1785/0120090367

Akkar S, Sandıkkaya MA, Bommer JJ (2014) Empirical ground-motion models for point- and extended-source crustal earthquake scenarios in Europe and the Middle East. Bull Earthq Eng 12:359–387. https://doi.org/10.1007/s10518-013-9461-4

Alavi E, Mahootchian A, Yadegari S, Shamsodin M, Babania Nouri M, Ordoubadi B (2018) Report of M7.3 Ezgele, Kermanshah, Iran Earthquake on November 12, 2017, EERI reports

Ambraseys NN, Melville CP (1982) A history of Persian earthquakes. Cambridge University Press, Cambridge. https://doi.org/10.1002/eqe.4290110412
ATC20 (1989) Procedures for post earthquake safety evaluation of buildings
Baker J, Jayaram N (2008) Correlation of spectral acceleration values from NGA ground motion models. Earthq Spectra 24:299–317
Bazzurro P, Cornell CA (2004) Nonlinear soil-site effects in probabilistic seismic-hazard analysis. Bull Seismol Soc Am 94:2110–2123
Bazzurro P, Luco N (2005) Accounting for uncertainty and correlation in earthquake loss estimation. In: Proceedings of the ninth international conference on structural safety and reliability, Rome, Italy, pp 2687–2694
Bazzurro P, Luco N (2007) Effects of different sources of uncertainty and correlation on earthquake-generated losses. Aust J Civ Eng. https://doi.org/10.1080/14488353.2007.11463924
Benjamin JR, Cornell CA (1970) Probability, statistics, and decision for civil engineers. McGraw-Hill, New York
Beygi S, Nadimi A, Safaei H (2016) Tectonic history of seismogenic fault structures in Central Iran. J Geosci 61:127–144
Boore DM, Stewart JP, Seyhan E, Atkinson GM (2014) NGA-West2 equations for predicting PGA, PGV, and 5% damped PSA for shallow crustal earthquakes. Earthq Spectra 30:1057–1085. https://doi.org/10.1193/070113eqs184m
Campbell KW, Bozorgnia Y (2014) NGA-West2 ground motion model for the average horizontal components of PGA, PGV, and 5% damped linear acceleration response spectra. Earthq Spectra 30:1087–1115. https://doi.org/10.1193/062913eqs175m
Cauzzi C, Faccioli E, Vanini M, Bianchini A (2015) Updated predictive equations for broadband (0.01–10 s) horizontal response spectra and peak ground motions, based on a global dataset of digital acceleration records. Bull Earthq Eng 13:1587–1612. https://doi.org/10.1007/s10518-014-9685-y
Chiou B-J, Youngs RR (2008) An NGA model for the average horizontal component of peak ground motion and response spectra. Earthq Spectra 24:173–215. https://doi.org/10.1193/1.2894832
Chiou BS-J, Youngs RR (2014) Update of the Chiou and Youngs NGA model for the average horizontal component of peak ground motion and response spectra. Earthq Spectra 30:1117–1153. https://doi.org/10.1193/072813eqs219m
Crowley H, Bommer JJ, Pinho R, Bird J (2005) The impact of epistemic uncertainty on an earthquake loss model. Earthq Eng Struct Dyn 34:1653–1685. https://doi.org/10.1002/eqe.498
Danciu L, Kale Ö, Akkar S (2016a) The 2014 earthquake model of the Middle East: ground motion model and uncertainties. Bull Earthq Eng. https://doi.org/10.1007/s10518-016-9989-1
Danciu L, Sesetyan K, Demircioglu M, Erdik M, Giardini D (2016b) OpenQuake input files of the seismogenic source model of the 2014 earthquake model of the Middle East (EMME-Project). https://doi.org/10.12686/a3
Danciu L et al (2017) The 2014 earthquake model of the Middle East: seismogenic sources. Bull Earthq Eng. https://doi.org/10.1007/s10518-017-0096-8
Douglas J, Edwards B (2016) Recent and future developments in earthquake ground motion estimation. Earth Sci Rev 160:203–219. https://doi.org/10.1016/j.earscirev.2016.07.005
Erdik M, Şeşetyan K, Demircioğlu MB, Hancılar U, Zülfikar C (2011) Rapid earthquake loss assessment after damaging earthquakes. Soil Dyn Earthq Eng 31:247–266. https://doi.org/10.1016/j.soildyn.2010.03.009
Erdik M, Sesetyan K, Demircioğlu M, Tüzün C (2012) Assessment of seismic hazard in the Middle East and Caucasus: EMME (Earthquake Model of Middle East) Project. Paper presented at the 15WCEE, 24–28 September, Lisbon, Portugal
Fallah Tafti M, Amini Hosseini K, Firouzi E, Mansouri B, Ansari A (2017) Ranking of GMPEs for seismic hazard analysis in Iran using LH, LLH and EDR approaches. J Seismol Earthq Eng 19:139–161
FEMA-P58 (2012) Federal Emergency Management Agency: Seismic Performance Assessment of Buildings, prepared by the Applied Technology Council for the Federal Emergency Management Agency, Washington, DC
Firuzi E, Ansari A, Amini Hosseini K, Rashidabadi M (2019) Probabilistic earthquake loss model for residential buildings in Tehran, Iran to quantify annualized earthquake loss. Bull Earthq Eng 17:2383–2406. https://doi.org/10.1007/s10518-019-00561-z
Ghasemi H, Zare M, Fukushima Y, Koketsu K (2009) An empirical spectral ground-motion model for Iran. J Seismol 13:499–515. https://doi.org/10.1007/s10950-008-9143-x
Ghodrati Amiri G, Razeghi HR, Razavian ASA, Aalaee H, Rasouli SM (2008) Seismic hazard assessment of Shiraz, Iran. J Appl Sci 8:38–48

Giardini D (1999) The Global Seismic Hazard Assessment Program (GSHAP)—1992/1999 1999 42. https://doi.org/10.4401/ag-3780

Goda K (2015) Seismic risk management of insurance portfolio using catastrophe bonds. Comput Aid Civ Infrastruct Eng 30:570–582. https://doi.org/10.1111/mice.12093

Goda K, Hong HP (2008) Estimation of seismic loss for spatially distributed buildings. Earthq Spectra 24:889–910. https://doi.org/10.1193/1.2983654

Goda K, Yoshikawa H (2012) Earthquake insurance portfolio analysis of wood-frame houses in southwestern British Columbia, Canada. Bull Earthq Eng 10:615–643. https://doi.org/10.1007/s10518-011-9296-9

Goda K, Wenzel F, Daniell J (2014) Insurance and reinsurance models for earthquake. In: Beer M, Kougioumtzoglou IA, Patelli E, Au IS-K (eds) Encyclopedia of earthquake engineering. Springer, Berlin. https://doi.org/10.1007/978-3-642-36197-5_261-1

ICSRDB (2014) Iranian code of practice for earthquake resistant design of buildings (Standard 2800), 4th edn. PN S 253, Building and Housing Research Center of Iran, Tehran

Jafari MK et al (2005) Seismic hazard study, final report for Tehran Comprehensive Plan. International Institute of Earthquake Engineering and Seismology (IIEES), Iran

Jaiswal K, Wald D (2013) Estimating economic losses from earthquakes using an empirical approach. Earthq Spectra 29:309–324. https://doi.org/10.1193/1.4000104

JICA (2000) The study on seismic microzoning of the greater Tehran area in the Islamic Republic of Iran, final report

Jonkman SN, van Gelder PHAJM, Vrijling JK (2003) An overview of quantitative risk measures for loss of life and economic damage. J Hazard Mater 99:1–30. https://doi.org/10.1016/S0304-3894(02)00283-2

Kale Ö, Akkar S, Ansari A, Hamzehloo H (2015) A ground-motion predictive model for Iran and Turkey for horizontal PGA, PGV, and 5% damped response spectrum: investigation of possible regional effects. Bull Seismol Soc Am 105:963–980. https://doi.org/10.1785/0120140134

Kamalian M, Jafari MK, Ghayamghamian MR, Shafiee A, Hamzehloo H, Haghshenas E, Sohrabi-bidar A (2008) Site effect microzonation of Qom, Iran. Eng Geol 97:63–79. https://doi.org/10.1016/j.enggeo.2007.12.006

Kohrangi M, Danciu L, Bazzurro P (2018) Comparison between outcomes of the 2014 Earthquake Hazard Model of the Middle East (EMME14) and national seismic design codes: the case of Iran. Soil Dyn Earthq Eng 114:348–361. https://doi.org/10.1016/j.soildyn.2018.07.022

Kohrangi M, Bazzurro P, Vamvatsikos D (2021) Seismic risk and loss estimation for building stock in Isfahan. Part I: exposure and vulnerability. Bulletin of Earthquake Engineering (**under review**)

Mansouri B, Ghafory-Ashtiany M, Amini-Hosseini K, Nourjou R, Mousavi M (2010) Building seismic loss model for Tehran. Earthq Spectra 26:153–168. https://doi.org/10.1193/1.3280377

Mansouri B, Kiani A, Amini-Hosseini K (2014) A platform for earthquake risk assessment in Iran case studies: Tehran scenarios and Ahar-Varzeghan earthquake. J Seismol Earthq Eng 16:51–69

Moinfar AA, Naderzadeh A, Nabavi MH (2012) New Iranian seismic hazard zoning map for new edition of seismic code and its comparison with neighbor countries. Paper presented at the 15th WCEE, Lisbon, Portugal

Motamed H, Calderon A, Silva V, Costa C (2019) Development of a probabilistic earthquake loss model for Iran. Bull Earthq Eng 17:1795–1823. https://doi.org/10.1007/s10518-018-0515-5

Park J, Bazzurro P, Baker JW (2007) Modeling spatial correlation of ground motion intensity measures for regional seismic hazard and portfolio loss estimation. Paper presented at the applications of statistics and probability in civil engineering—Kanda, Takada & Furuta (eds)

Sadeghi M, Hochrainer-Stigler S, Ghafory-Ashtiany M, Pakdel-Lahiji N (2014) Earthquake risk modeling for the evaluation of losses to property owners in the metropolitan area of Shiraz. In: Proceedings of the 10th U.S. national conference in earthquake engineering. Earthquake Engineering Research Institute, Anchorage, AK

Sadeghi M, Hochrainer-Stigler S, Ghafory-Ashtiany M (2015) Evaluation of earthquake mitigation measures to reduce economic and human losses: a case study to residential property owners in the metropolitan area of Shiraz, Iran. Nat Hazards 78:1811–1826. https://doi.org/10.1007/s11069-015-1801-z

Safaei H (2005) Identify and evaluate the seismic potential of faults around Isfahan. Final report of the research project, University of Isfahan (in Farsi)

Safaei H, Tabatabaeimanesh SM, Hashemi SN, Mirlohi AS, Vafa H (2012) Structural and petrological evidence for the continuation of the Isfahan fault system across the Urumieh-Dokhtar zone of central Iran. Geotectonics 46:455–471. https://doi.org/10.1134/s0016852112060064

Sandıkkaya MA, Akkar S, Bard P-Y (2018) A probabilistic procedure to describe site amplification factors for seismic design codes. Soil Dyn Earthq Eng. https://doi.org/10.1016/j.soildyn.2018.01.050

Şeşetyan K et al (2018) The 2014 seismic hazard model of the Middle East: overview and results. Bull Earthq Eng. https://doi.org/10.1007/s10518-018-0346-4
Shafiee A, Kamalian M, Jafari MK, Hamzehloo H (2011) Ground motion studies for microzonation in Iran. Nat Hazards 59:481–505. https://doi.org/10.1007/s11069-011-9772-1
Silva V (2019) Uncertainty and correlation in seismic vulnerability functions of building classes. Earthq Spectra 35:1515–1539. https://doi.org/10.1193/013018EQS031M
Silva V, Crowley H, Pagani M, Monelli D, Pinho R (2014) Development of the OpenQuake engine, the Global Earthquake Model's open-source software for seismic risk assessment. Nat Hazards 72:1409–1427. https://doi.org/10.1007/s11069-013-0618-x
Tajmir Riahi Z, Ajalloeian R, Rahgozar MA, Safaei H (2014) Earthquake hazard zonation of the Isfahan City, Iran. J Geotech Eng 19:7141–7163
Vernant P et al (2004) Deciphering oblique shortening of central Alborz in Iran using geodetic data. Earth Planet Sci Lett 223:177–185. https://doi.org/10.1016/j.epsl.2004.04.017
Wair B, DeJong JT, Shantz T (2012) Guidelines for estimation of shear wave velocity profiles. PEER 2012/08
Wald DJ, Allen TI (2007) Topographic slope as a proxy for seismic site conditions and amplification. Bull Seismol Soc Am 97:1379–1395. https://doi.org/10.1785/0120060267
Weatherill GA, Silva V, Crowley H, Bazzurro P (2015) Exploring the impact of spatial correlations and uncertainties for portfolio analysis in probabilistic seismic loss estimation. Bull Earthq Eng 13:957–981. https://doi.org/10.1007/s10518-015-9730-5
Whitehead J, Rose A (2009) Estimating environmental benefits of natural hazard mitigation with data transfer: results from a benefit-cost analysis of Federal Emergency Management Agency hazard mitigation grants. Mitig Adapt Strat Glob Change 14:655–676. https://doi.org/10.1007/s11027-009-9189-2
Yazdi-Samadi MR, Mahsuli M (2018) Time-variant seismic risk analysis of transportation networks considering economic and socioeconomic impacts. J Earthq Eng. https://doi.org/10.1080/13632469.2018.1453401
Zafarani H, Mousavi M (2014) Applicability of different ground-motion prediction models for northern Iran. Nat Hazards 73:1199–1228. https://doi.org/10.1007/s11069-014-1151-2
Zafarani H, Hajimohammadi B, Jalalalhosseini SM (2017) Earthquake hazard in the Tehran region based on the characteristic earthquake model. J Earthq Eng. https://doi.org/10.1080/13632469.2017.1387189
Zare M (2010) Fundamental of seismic hazard analyses. Intern Inst Earthq Eng Seism (IIEES), in Persian, Tehran, Iran
Zare M (2015) Probabilistic seismic hazard zoning in Iran: a state of the art on the studies during four decades. Paper presented at the 7th international conference on seismology & earthquake engineering, Tehran, 18–21 May
Zare M et al (2014) Recent developments of the Middle East catalog. J Seismol 18:749–772. https://doi.org/10.1007/s10950-014-9444-1
Zhao JX et al (2006) Attenuation relations of strong ground motion in Japan using site classification based on predominant period. Bull Seismol Soc Am 96:898–913. https://doi.org/10.1785/0120050122
Zhao J, Lee JY, Li Y, Yin Y-J (2019) Effect of catastrophe insurance on disaster-impacted community: Quantitative framework and case studies. Int J Disaster Risk Reduct 43:101387. https://doi.org/10.1016/j.ijdrr.2019.101387
Zolfaghari MR (2010) Application of catastrophe loss modelling to promote property insurance in developing countries. Disasters 34:524–541. https://doi.org/10.1111/j.1467-7717.2009.01141.x